ACS Catalysis

pubs.acs.org/acscatalysis

Research Article

Three-Stage Conversion of Chemically Inert *n*-Heptane to *α*-Hydrazino Aldehyde Based on Bioelectrocatalytic C−H Bond Oxyfunctionalization

N. Samali Weliwatte,[†] Hui Chen,*[,†] Tianhua Tang, and Shelley D. Minteer*

Cite This: *ACS Catal.* 2023, 13, 563−572

Read Online

ACCESS | Metrics & More | Article Recommendations | Supporting Information

ABSTRACT: Simple petrochemical feedstocks are often the starting material for the synthesis of complex commodity and fine and specialty chemicals. Designing synthetic pathways for these complex and specific molecular structures with sufficient chemo-, regio-, enantio-, and diastereo-selectivity can expand the existing petrochemicals landscape. The two overarching challenges in designing such pathways are selective activation of chemically inert C−H bonds in hydrocarbons and systematic functionalization to synthesize complex structures. Multienzyme cascades are becoming a growing means of overcoming the first challenge. However, extending multienzyme cascade designs is restricted by the arsenal of enzymes currently at our disposal and the compatibility between specific enzymes. Here, we couple a bioelectrocatalytic multienzyme cascade to organocatalysis, which are two distinctly different classes of catalysis, in a single system to address both challenges. Based on the development and utilization of an anthraquinone (AQ)-based redox polymer, the bioelectrocatalytic step achieves regioselective terminal C−H bond oxyfunctionalization of chemically inert *n*-heptane. A second biocatalytic step selectively oxidizes the resulting 1-heptanol to heptanal. The succeeding inherently simple and durable L-proline-based organocatalysis step is a complementary partner to the multienzyme steps to further functionalize heptanal to the corresponding *α*-hydrazino aldehyde. The "three-stage" streamlined design exerts much control over the chemical conversion, which renders the collective system a versatile and adaptable model for a broader substrate scope and more complex C−H functionalization.

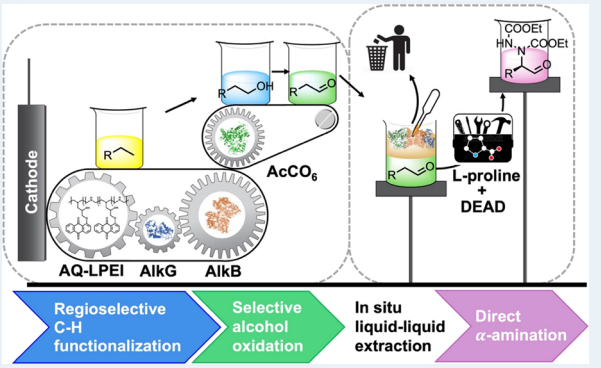

KEYWORDS: *C−H activation, redox polymer-mediated, hybrid bioelectrocatalysis, in vitro multienzyme cascade, organocatalysis, tandem catalysis*

INTRODUCTION

The petrochemicals industry systematically converts simple, ubiquitous, and chemically inert hydrocarbons to consistently more complex, and, therefore, functionally more valuable intermediates, commodity, and fine and specialty chemicals indispensable to everyday life.[1] Petrochemical feedstock accounts for approximately 12% of the global oil demand, and the estimated value of the petrochemicals industry at over $500 billion (2022) is projected to grow steadily through the next decade.[2] While the deep conversion and comprehensive utilization of chemically inert hydrocarbons are an increasingly viable platform for molecular synthesis to diversify the existing petrochemicals product landscape, there are two major challenges to be addressed. The first is the arduous functionalization of unpolarized aliphatic C−H bonds, which are intrinsically inert due to high bond dissociation energies (BDEs).[1,3,4] The second is the design and construction of flexible and sustainable routes to effectively realize these complicated conversions with minimum negative environmental impact.

Industrial cracking processes, transition metal-based or radical-mediated pathways remain the mainstream methods of C−H bond functionalization.[4−6] The energy intensity and harsh reaction conditions (e.g., high temperatures and pressures, precious metals, and toxic species) employed therein limit chemoselectivity (i.e., overoxidation and byproducts) and regioselectivity, particularly in activating terminal C−H bonds, which have higher BDEs compared to internal sites (e.g., BDEs 101.4 vs 98.8 kCal mol^{-1} in *n*-heptane).[4,5,7,8] Alternatively, enzymatic C−H bond functionalization is highly chemo- and regioselective and substrate specific, uses clean oxidants (e.g., O_2), operates under mild physiological conditions in aqueous

Received: August 12, 2022
Revised: November 12, 2022
Published: December 22, 2022

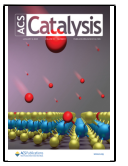

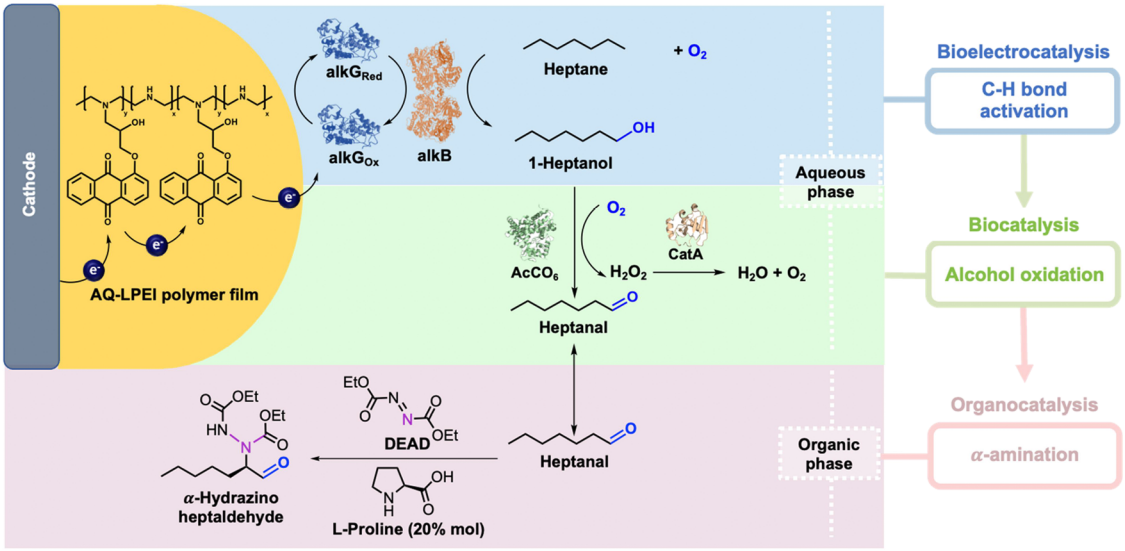

Figure 1. Schematic representation of the "three-stage" hybrid bioelectro-organocatalytic strategy for the sequential; regioselective C−H functionalization in *n*-heptane, selective oxidation of 1-heptanol, and α-amination.

media, and shows significantly superior catalytic rates per active site compared to transition metal catalysts.[8−12] In vitro multienzyme cascades implement high atom economy, chemo-, regio-, diastereo-, and enantioselectivity, low operational time, low environmental impact, and evade intermittent intermediate purification (i.e., "synthetic ideality") during deep conversions.[13−15] For example, Yu et al. used a multienzyme cascade to enantioselectively functionalize phenylethane to an amine concomitant to cofactor regeneration.[16] Electroenzymatic cascades further streamline systems for C−H functionalization by providing controlled reductive energy via an electrode instead of stoichiometric amounts of expensive cofactors, and powering through sluggish kinetics.[11] For example, Yuan et al. reported an electroenzymatic cascade of rubredoxin (alkG) and alkane monooxygenase (alkB) for regioselective oxyfunctionalization of alkanes and alkenes.[17] Chen et al. designed an elaborate electroenzymatic cascade for the sequential conversion of alkanes to corresponding primary alcohols, aldehydes, and eventually imines.[18]

One major design limitation in electroenzymatic routes is the poor electrochemical communication between electrodes and enzymes. The rate of direct electron transfer (DET) by tunneling at the cathode−enzyme interface is limited by the spatial distribution of enzymes (i.e., distance to the electrode, relative concentration, and orientation on the electrode) based on Marcus theory.[19,20] Therefore, mediated electron transfer (MET) by redox entities is critical to reduce contact resistance, shuttle electrons between the cathode and enzymes, and increase synthetic output.[11] Toluidine blue O (TBO) and neutral red (NR) used in electroenzymatic alkane oxyfunctionalization[17,18] and ferrocene and Ru-based molecules used in polarized C(sp^3)−H bond functionalization[21] are such common diffusible redox mediators. These redox species are homogenously dispersed in the catalytic media, which (i) require high concentrations to facilitate electron transfer, (ii) complicate eventual product isolation and waste disposal, and (iii) are typically ecotoxic. Conversely, localized redox polymer hydrogels and 3D matrices "trap" redox centers, enzymes, and substrates at the electrode vicinity increasing effective interactions for charge and mass transfer.[11,22,23] Phase separation between the biocatalytic media and spatially constricted redox polymer eases eventual product isolation from the system and waste processing (i.e., heterogeneous catalytic features). Unlike with diffusible mediators, MET kinetics of redox polymers can be modulated by their operational parameters (e.g., redox polymer thickness and quality) and intrinsic parameters (e.g., diffusion coefficient and partition coefficient).[24] Some redox polymers embody additional case-specific functionalities, such as enzymatic activation, protection (against oxygen damage, high potential deactivation, and cytotoxicity), and electrode sensitivity to external triggers (e.g., light, pH, and temperature).[25,26] However, the use of redox polymers in electroenzymatic value-addition of C_n species has hitherto largely involved electrosynthetic CO_2 reduction.[22,27−29]

Other design limitations in multienzyme cascades include (i) incompatibility between certain enzymes and (ii) unavailability of specific enzymes required in biocatalytic retrosynthetic routes. To realize such complicated catalytic transformations and integrate the advantages of different catalytic methods, hybrid cascade designs of single enzymes coupled to molecular catalysts or photocatalysts are on the rise.[30−33] For example, Denard et al. reported the cooperative tandem use of the Grubb's catalyst and cytochrome P450 for C(sp^2)−H functionalization into enantioselective aliphatic and aryl epoxides.[30,34] C−H bonds have been functionalized to chiral diols in excellent yield and stereoselectivity by coupling laccase or alcohol dehydrogenase to organocatalysis.[35] Tandemly-used enzymes and photocatalysts (e.g., porphyrins and sodium AQ-2-sulfonate) have been reported for C−H hydroxylation, halogenation, amination, and ketone formation.[36] Cai et al. reported a cytochrome P450-mimetic metal organic framework that works in tandem with dehydrogenases, which is a photo-, chemo-, and biocatalytic hybrid, for C(sp^2)−H functionalization.[37]

In this study, we report a "three-stage (bioelectrocatalysis−biocatalysis−organocatalysis)" system that couples a bioelectrocatalytic multienzyme cascade with single amino acid-based organocatalysis for the sequential functionalization of *n*-heptane to 1-heptanol, heptanal, and eventually the corre-

https://doi.org/10.1021/acscatal.2c04003
ACS Catal. 2023, 13, 563−572

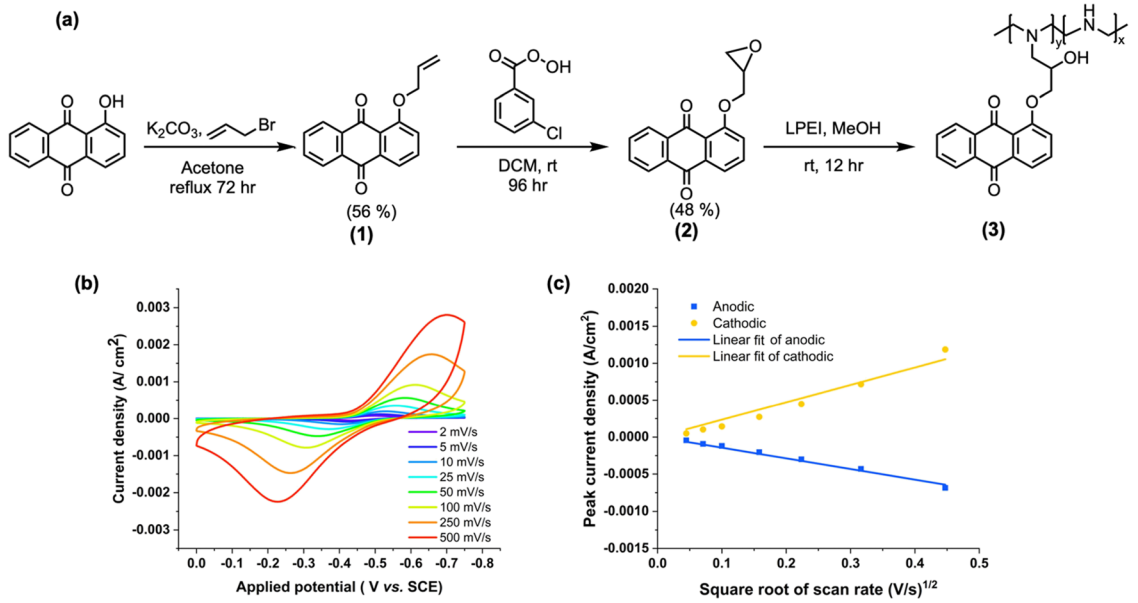

Figure 2. (a) Scheme: synthetic pathway of the AQ-LPEI polymer. (b) Representative CVs of a carbon paper electrode modified with the AQ-LPEI redox hydrogel. Electrolyte: Kpi buffer at pH 8.0, including 50 mM NaCl and 15% glycerol. Scan rates 2−500 mV s^{-1}. (c) Linear fit of the square root of scan rate vs peak current.

sponding α-hydrazino aldehyde (Figure 1). The cathodic chamber contains an alkane monooxygenase (alkB, E C 1.14.15.3) from *Pseudomonas putida* GPO1,[38] a rubredoxin (alkG) protein from *P. putida* GPO1,[38] an engineered choline oxidase ($AcCO_6$, E C 1.1.3.17) from *Arthrobacter chlorophenolicus*,[39] and a catalase (CatA, EC 1.11.1.6) from *Bacillus subtilis*.[40] Sequential bioelectrocatalytic C−H bond functionalization (step I) mediated by an immobilized new anthraquinone-linear polyethyleneimine (AQ-LPEI) redox polymer, biocatalytic alcohol oxidation (step II), and organocatalytic α-amination (step III) manifest the "synthetic ideality" and quintessential advantages of multienzyme and bioelectrocatalytic systems to address the common challenges encountered during deep conversion of paraffinic hydrocarbons (vide supra). The eventual α-hydrazino aldehyde is a platform chemical that can be converted to extremely useful α-amino-aldehyde and acid equivalents by facile reductive N−N bond cleavage.[41−43]

RESULTS AND DISCUSSION

During the functionalization of unpolarized terminal C−H bonds in *n*-heptane (step I), the new AQ-LPEI redox polymer establishes electrochemical communication at the cathode-alkG interface. Additionally, compared to common diffusible redox mediators used in this applicational context,[17,18] the spatial constriction of AQ-LPEI on the cathode (i.e., heterogenous catalytic mediation) and the nonuse of stoichiometric amounts of reductive cofactors or sacrificial substrates in the system design collectively assist the extraction of heptanal in step II from an assortment of enzymes in aqueous media into an organic phase for the organocatalytic step III.

Synthesis, Characterization, and Redox Mediation of AQ-LPEI Redox Polymer Hydrogel. The AQ-LPEI consists of a 9,10-AQ pendant, a linear polyethyleneimine (LPEI) backbone, and a linker arm. The rationale behind selecting the AQ pendant is fourfold. First, the reductive potential of alkG (−0.24 V vs SCE) is within the range of many AQ moieties, rendering sequential electron transfer from AQ mediator to alkB via alkG, and thermodynamically feasible.[18,44,45] Second, AQ moieties undergo extremely rapid and reversible two-proton-coupled two-electron transfer mechanisms especially in aqueous media (Scheme S1).[44,46] Resultantly, the rich redox chemistry of AQs extends to microbial fuel cells, redox flow batteries, solar cell devices, redox-dyes, antioxidants, antitumor agents, molecular electronics, wastewater treatment, and other energy storage systems.[44,46−49] Third, quinones, as natural electron acceptors/donors in key biological processes (e.g., photosynthesis, neurotransmission, and cellular signaling), are typically biocompatible and nontoxic to most biocatalysts.[50,51] Quinones have good biocatalytic redox active site accessibility because the quinone/hydroquinone redox function occurs across membranes or interfaces.[52] Finally, AQs are relatively small, prototypically hydrophobic, and aromatic polyketide rings.[53] The high partition coefficient of AQs in hydrophobic media is postulated to increase its affinity toward the hydrophobic core of small globular proteins, and the organic substrate in aqueous media. Naphtho- and anthraquinones form covalent interactions with thiol, amine, and hydroxyl groups in enzymes establishing "contact" at the enzyme-terminal.[26,54] The aromatic pendants parallelly π-stack with the graphene in carbon paper establishing "contact" at the electrode-terminal.[55] In terms of the backbone, PEI is a water-insoluble, polycationic polymer with one of the highest positive charge density potentials due to every third atom being a protonatable amine.[56] Therefore, LPEI forms hydrogels facilitating redox polymer swelling and rapid substrate diffusion on the electrode.[57] The linker arm connects the pendant to the backbone and provides a conditional mobility (i.e., "bounded diffusion model") as a function of linker length for redox shuttling.[58] The $(-O-CH_2-CH(OH)-CH_2^-)$ linker was chosen based on the facile reactivity between amines (i.e., LPEI) and epoxides (**2**) in forming AQ-LPEI (Figure 2a).[59] This linker has also been shown to elicit conditional mobility to quinone pendants.[59]

https://doi.org/10.1021/acscatal.2c04003
ACS Catal. 2023, 13, 563−572

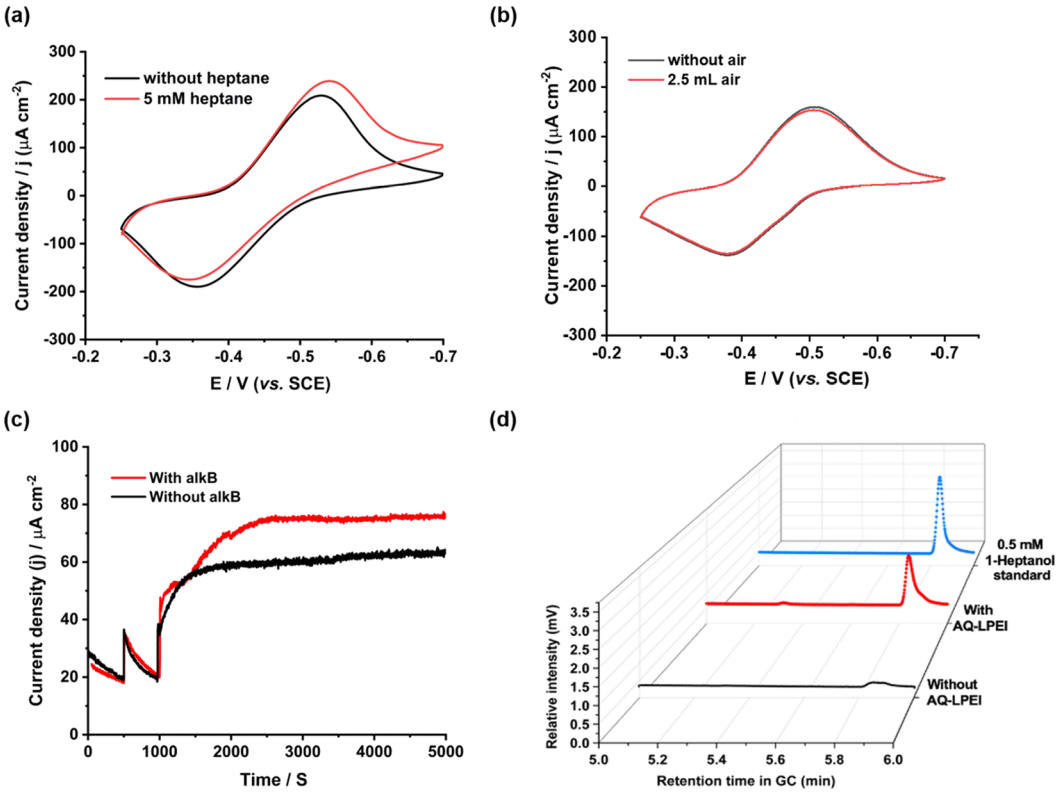

Figure 3. (a) Representative CVs for the alkB/alkG bioelectrocatalysis mediated by the AQ-LPEI redox polymer-immobilized electrode in the presence (red curve) and absence (black curve) of 5 mM heptane (3% in acetone cosolvent). Electrolyte: 0.09 U/mL (0.18 mg/mL) alkB, 0.78 mg/mL alkG (molar ratio of alkB to alkG = 1:10), and 50 mM Kpi buffer (pH 8.0) containing 50 mM NaCl and 15% glycerol. Scan rates 5 mV s^{-1}. A volume of 2.5 mL of air (36% headspace volume) was injected into the anaerobic three-electrode system. (b) Representative CVs for the AQ-LPEI redox polymer-immobilized electrode in the presence (red curve) and absence (black curve) of 2.5 mL of air (36% headspace volume) injected into the anaerobic three-electrode system. Electrolyte: 50 mM Kpi buffer (pH 8.0) containing 50 mM NaCl and 15% glycerol. Scan rates 5 mV s^{-1}. (c) Amperometric *i*−*t* analysis of the alkB/alkG bioelectrocatalytic system in the presence (red curve) and absence (black curve) of 0.09 U/mL (0.18 mg/mL) alkB. The reaction was performed in an anaerobic H-shaped cell while stirring. 3 mL of catholyte: 0.78 mg mL^{-1} alkG (molar ratio of alkB to alkG = 1:10) and 50 mM Kpi buffer (pH 8.0) containing 50 mM NaCl and 15% glycerol. Applied potential −0.8 V vs SCE. Substrates, 5 mM heptane (3% in acetone cosolvent), and 2.5 mL of air (36% headspace volume) were sequentially injected to the anaerobic cathode chamber. The electrolyte was gently stirred at 850 rpm. Anode chamber contained saturated KCl, Pt (counter), and saturated calomel (reference) electrodes. (d) Representative GC analysis for the formation of 1-heptanol by the bulk electrolysis conducted in step I in the presence (red curve) and absence (black curve) of AQ-LPEI redox polymer.

The rate of electron self-exchange across the redox polymer and the rate of heterogeneous electron transfer at the electrode-enzyme interface are functions of the choice of redox moiety and their spacing.[25] The percent substitution of AQ pendants in the LPEI backbone, which is inversely proportional to the spacing, was determined independently by nuclear magnetic resonance (^{1}H NMR) (Figure S1) and X-ray photoelectron spectroscopy (XPS) (Figures S2 and S3). Interestingly, the substitution in AQ-LPEI (∼87−88%) is approximately 4- and 18-times higher compared, respectively, to analogous naphthoquinone-4-LPEI and naphthoquinone-2-LPEI redox polymers.[59] This higher pendant substitution in AQ-LPEI is attributive to the higher electron density on AQ, which better stabilizes the partial positive charge on oxygen as opposed to naphthoquinone in the transition state formed between anthraquinone glycidol and LPEI during nucleophilic substitution (Figure 2a).

Electrochemical characterization of AQ-LPEI immobilized on carbon paper via cyclic voltammetry (Figure 2b) recorded a formal redox potential (E^{01}) of −0.466 V vs SCE. The cathodic to anodic peak-to-peak separation (ΔE) varies with scan rate indicative of free "diffusion-like" electron conduction across the AQ-LPEI film in the electrode surface vicinity. The anodic to cathodic peak current ratio is lower than 1 (i.e., higher kinetic barrier to oxidative electron transfer), which corroborates the quasi-reversibility of proton-coupled electron transfer characteristic to benzoquinones.[60] Self-exchange-based electron transfer through redox hydrogels is typically quantified via the apparent electron diffusion coefficient (D_{app}), which is a function of the structure of the redox polymer (specifically, the length/mobility of the linker, distance and mobility of the redox moieties, etc.).[51,59,61] The D_{app} for AQ-LPEI immobilized on a carbon paper electrode was determined using the Randles−Ševčík equation (eq S1) (Figure 2c). Assuming that (i) the concentration of AQ-LPEI in the drop cast volume is approximately unchanged on the porous carbon paper upon drying and subsequently absorbing aqueous electrolyte and (ii) two electrons participate in the rate-determining redox reaction, the D_{app} for AQ-LPEI polymer was estimated as 1.1 ± 0.5 × 10^{-8} cm^2 s^{-1}. This value is closer in range to D_{app} values of transition metal-containing redox polymers (∼ ×10^{-8} cm^2 s^{-1})[27] than fully organic counterparts (∼10^{-12} to 10^{-11} cm^2 s^{-1}) determined using the Randles−Ševčík method.[51,59,62] The high D_{app} is attributed to the rapid and reversible kinetics

https://doi.org/10.1021/acscatal.2c04003
ACS Catal. 2023, 13, 563−572

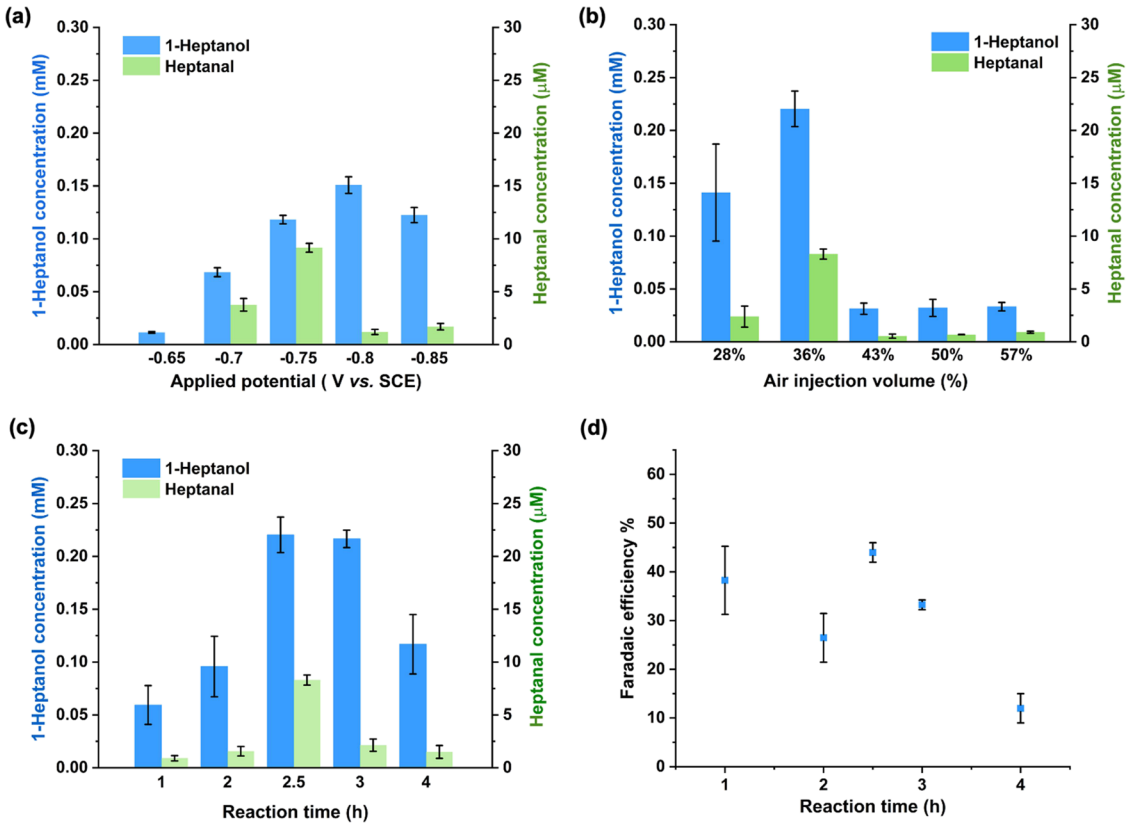

Figure 4. Optimization of (a) applied potential (reaction time is 2.5 h), (b) air injection volume (as a % of 7 mL headspace volume and reaction time is 2.5 h), (c) reaction time, and (d) faradaic efficiency for the bioelectrocatalytic step I of converting *n*-heptane to 1-heptanol. All experiments were conducted in anaerobic H-cells while stirring. Electrolyte: 3 mL of 50 mM Kpi buffer (pH 8.0) containing 0.09 U/mL (0.18 mg/mL) alkB, 0.78 mg/mL alkG (molar ratio of alkB to alkG = 1:10), 50 mM NaCl, and 15% glycerol.

of two-proton-coupled two-electron transfer mechanisms of AQ in aqueous media,[44,46] and the relatively high percentage of AQ pendant substitution onto the LPEI backbone leading to rapid electron self-exchange between proximal π-stacked AQ moieties (vide supra). Therefore, the flux of reductive energy channeling through the AQ-LPEI polymer, eventually to be mediated to the enzyme cascade during electrocatalysis, is significantly high.

Step I: Bioelectrocatalytic Regioselective C−H Bond Oxyfunctionalization. C−H bond functionalization in step I is catalyzed by alkB in the catholyte. AlkB is known for its rare ability to regioselectively functionalize inert terminal C−H bonds in gasoline range alkanes (C_5−C_{12}).[18] In native bacterial systems, the reductive energy required by alkB originates from NADH-dependent rubredoxin reductase (alkT) and transfers to alkB via the electron transfer protein alkG.[12] In the reaction system of this study, the cathode supplies reductive energy to alkB via alkG, deeming the need for alkT and sacrificial substrate/enzyme-dependent regeneration methods for the NADH cofactor redundant.[17,18] The AQ-LPEI polymer is used to mediate the cathode-to-alkG-to-alkB reductive energy transfer.

In previous studies of bioelectrocatalytic systems, biocatalysts (i.e., alkB) and diffusible redox mediators (e.g., TBO[17] or NR[18]) that shuttle electrons from the electrode to alkG are all injected to the electrolyte. The reported molar ratio of alkB:alkG in such electrolytes was 1:1. The electron mediator in the present study is the polymer AQ-LPEI, immobilized on the electrode surface, which spatially restricts its redox mediating capabilities to the vicinity of the electrode surface. This spatial restriction of the AQ-LPEI redox mediator was compensated by using a higher fraction of alkG in the electrolyte than 1:1 because alkG is the immediate electron acceptor from AQ-LPEI. It was also assumed that a higher fraction of alkG over alkB would implement catalytically effective interactions of alkG with AQ-LPEI without hindering electron hopping across AQ-LPEI in the presence of alkB. Therefore, the molar ratio of alkB:alkG in the present study was 1:10.

The anticipated redox mediation by AQ-LPEI at the electrode-enzyme interface was verified by cyclic voltammetry as shown in Figure 3a. In the three-electrode system containing substrates *n*-heptane, O_2, alkG, and alkB (red curve), a catalytic peak onset of E^{01} of AQ-LPEI (−0.46 V vs SCE) is observed, compared to nonturnover conditions without heptane (black curve), indicating an electrocatalytic reduction mediated by AQ-LPEI. The reductive catalytic peak appears around the reductive potential of AQ-LPEI at −0.53 V vs SCE.Control cyclic voltammograms (CVs) (Figure 3b) for the AQ-LPEI immobilized working electrode, in the presence (red curve) and absence of O_2 (black curve), indicate that the observed catalytic activity is not a result of an auxiliary reaction between the quinone moieties in AQ-LPEI and O_2. Amperometric i−t curves under bulk electrolysis conditions indicate that catalytic current generation in the presence of all substrates and reductive energy relies on the biocatalyst (i.e., alkB) (Figure 3c, red trace). A slight residual current is observed in the catalytic system upon the injection of air in the absence of alkB

https://doi.org/10.1021/acscatal.2c04003
ACS Catal. 2023, 13, 563−572

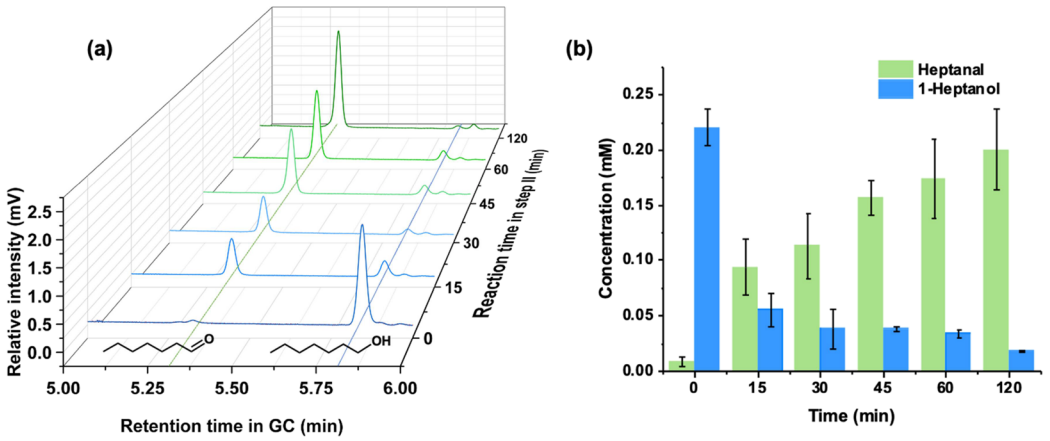

Figure 5. (a) Representative GC fragment analysis and (b) concentration profiles of 1-heptanol to heptanal conversion obtained by bulk electrolysis during the biocatalytic step II as a function of reaction time. The concentration of $AcCO_6$ is 0.14 U/mL (0.83 mg/mL) in 3 mL of reaction solution.

(black trace) due to the reduction of aqueous O_2 to H_2O_2 by reduced dihydroanthraquinone moieties in AQ-LPEI.[63] Gas chromatography (GC) analyses (Figure 3d) of the electrolyte after bulk electrolysis with an AQ-LPEI-modified cathode (red trace) confirm that the bioelectrocatalytic reduction mediated by AQ-LPEI is *n*-heptane conversion to 1-heptanol. The consequent 1-heptanol concentration in the H-cell was approximately 40-fold higher compared to a system with a bare cathode (black trace). Therefore, AQ-LPEI is mediating bioelectrocatalysis successively with alkG and alkB. The presence of AQ-LPEI in the catalytic system is imperative for regioselective bioelectrocatalytic conversion of *n*-heptane to 1-heptanol in step I. A control experiment in the absence of alkG showed no bioelectrocatalytic 1-heptanol generation (Figure S8) reflective of the literature precedence that establishes alkG as an indispensable component for electron transfer to alkB.

The performance of the bioelectrocatalytic step was further optimized in terms of applied potential, air injection volume, and reaction time (Figure 4). The applied potential is the driving force of the electrocatalytic element in step I. While an applied potential of −0.24 V vs SCE would theoretically suffice for thermodynamically feasible electron transfer from AQ-LPEI (reductive peak potential at approximately −0.53 V vs SCE) to alkG (−0.24 V vs SCE) to alkB to heptane, the rate of this reduction relies on overpotential (η). The applied potential of −0.8 V vs SCE recorded the highest concentration of 1-heptanol (0.15 ± 0.01 mM) during the bulk electrolysis for 2.5 h (Figure 4a). Low conversion rates at lower applied potentials are attributed to the sluggish electron transfers at the cathode-polymer-enzyme juncture. Low conversion rate at the higher applied potential (i.e., −0.85 V vs SCE) is attributed to increasing overpotential causing overreduction and ionization of AQ-LPEI. The polymer is possibly desorbed due to diminished hydrophobicity.[63,64] Optimizing the air injection volume in the H-cell headspace strikes a balance between (i) substrate availability for the bioelectrocatalytic O_2 reduction to 1-heptanol, (ii) undesirable proclivity for O_2 reduction to H_2O_2, and (iii) oxidation of the AQ moiety causing the degradation of AQ-LPEI overtime. An air injection volume of 2.5 mL (corresponding to 36% of volume in the hitherto anaerobic headspace of the cathode chamber) recorded the highest concentration of 1-heptanol (0.22 ± 0.02 mM) during 2.5 h of bulk electrolysis (Figure 4b). The drastic decline of 1-heptanol in systems with air injection volumes above 40% is attributed to the oversaturation of O_2 content in the headspace leading to the dominance of anthraquinone-mediated O_2 reduction to H_2O_2. Bulk electrolysis for a duration of 2.5 h recorded the highest 1-heptanol (0.22 ± 0.02 mM) formation (Figure 4c). Shorter durations resulted in lower yields as reaction time is a measure of the charge available for consumption during bulk electrolysis ($Q = it$). Longer durations also resulted in lower yields, possibly due to alcohol evaporation to the headspace in the stirring system.[18] The faradaic efficiency of the optimized bioelectrocatalytic step I of 44% at 2.5 h is highly competitive to existing reports of bioelectrocatalytic alkane oxyfunctionalization systems that utilize diffusible redox mediators (Figure 4d). For example, Yuan et al. recorded a faradic efficiency of 25 ± 1% for an alkB/alkG biocathode with TBO.[17] Chen et al. recorded a faradic efficiency of 45% for a bioelectrocatalytic system with alkB, alkG, and NR in the electrolyte apexing only after 4 h of operation.[18] The faradaic efficiency of the present study decreases with time possibly due to the competition between terminal C−H bond functionalization and O_2 reduction to H_2O_2.[63]

Step I achieved AQ-LPEI polymer-mediated regioselective bioelectrocatalytic C−H bond oxyfunctionalization via a multiprotein electron transfer pathway. As seen, the ability to easily variate and control the product profile as functions of electric energy input, charge (i.e., time), and reactants (e.g., injected air volume) renders bioelectrocatalytic systems an attractive synthetic option.

Step II: Biocatalytic Oxidation of 1-Heptanol to Heptanal. Selective oxidation of primary alcohols to aldehydes, evading the overoxidation to acids and esters, consistently remains a challenge in molecular synthesis.[65,66] Corresponding conventional organic synthetic routes require (i) stoichiometric amounts of harsh and/or toxic oxygen donors (e.g., MnO_2, Cr(IV), and Dess−Martin periodinane) that suffer from high cost and functional group incompatibility and generate significant quantities of byproducts or (ii) precious metal catalysts (Pt, Pd, Au, Ru, and Ti) that suffer from low selectivity or activity for the oxidation of aliphatic primary alcohols compared to aromatic and activated allylic alcohols.[65−67]

https://doi.org/10.1021/acscatal.2c04003
ACS Catal. 2023, 13, 563−572

In step II, bioelectrocatalytically synthesized 1-heptanol is enzymatically oxidized to heptanal. Enzymatic alcohol oxidation is more commonly facilitated by $NAD(P)^+$-dependent alcohol dehydrogenases (ADHs). Instead, an engineered choline oxidase variant, developed by Turner's group, with higher primary alcohol oxidase activity ($AcCO_6$) compared with the wild type enzyme was used in this study.[18,39] $AcCO_6$ sidesteps the use of expensive cofactors, cofactor regeneration, and potential interferences by the cofactor to eventual steps. The catalytic conditions were tuned for step II after 2.5 h of bulk electrolysis (step I) by (i) ceasing the applied potential, (ii) injecting $AcCO_6$, and (iii) altering the O_2 content in the headspace (see Experimental Section for electrochemical methods in the Supporting Information). Monitoring the concentration of 1-heptanol and heptanal as a function of time via GC (Figure 5) records a substrate conversion ratio of 91% (corresponding to 0.20 ± 0.02 mM heptanal) in 2 h with O_2 as oxidant. The catalase was injected into the system to scavenge byproduct, H_2O_2 (Figure 1). The optimized applied potential, air injection volume, and reaction time combination for the formation of 1-heptanol also results in the formation of a significant fraction of heptanal (Figure 4). This aldehyde formation has been commonly observed with alkG and alkB due to bioelectrocatalytic overreduction of alkane and primary alcohol under optimal conditions.[17,18]

Step III: Organocatalytic α-Hydrazino Aldehyde Formation. Aldehydes are precursors for the de novo synthesis of α-amino aldehydes and the primary source of chiral substrates used in stereoselective synthesis of amino acids, peptides, and proteins.[68] In step III, heptanal is α-aminated to the corresponding α-hydrazino aldehyde. Although theoretically feasible, extending a cascade of multienzymes is complex due to the specific substrate, cofactor, pH, and other physiological requirements of each enzyme, which can potentially interfere with the sequential activity and reaction flux of complex enzymes.[13,32,33] Accordingly, instead of an additional enzyme(s), a single chiral amino acid was used as the stereoselective catalyst for organocatalytic amination. As a proof of concept of the versatility and the adaptability of our system, heptanal in buffer was extracted to an organic phase for step III and wherein the widely reported L-proline catalyzed and direct asymmetric α-amination pathway was conducted.[43,69,70] Proline-based catalysis is stable, durable, and relatively unimpaired by interferences (e.g., residual buffer, salts, and glycerol in the organic phase following a liquid−liquid extraction) and not moisture-sensitive like analogous classical metal catalysts.[71]

In situ liquid−liquid extraction of heptanal in buffer to an organic phase such as acetonitrile was ineffective due to the water miscibility of acetonitrile. Salt-assisted liquid−liquid extraction of heptanal in aqueous electrolyte to acetonitrile proved practically onerous due to the small scale of the setup and the interference by high concentrations of residual salt (e.g., NaCl, $MgSO_4$, or Na_2CO_3) in acetonitrile. Therefore, dichloromethane (DCM) was used as the organic phase for extraction and solvent in step III. In step III, direct organocatalytic asymmetric α-amination of aldehydes reported by Bøgevig et al. was adapted for the conversion of extracted heptanal.[70] Interestingly, formation of α-hydrazino aldehyde (73%) after the heptanal extraction from the aqueous buffer is significantly higher than the same conversion conducted using a 0.20 mM heptanal stock solution in purely DCM that sidesteps the liquid−liquid extraction (35%) (Figure 6, Table S1). This is attributed to the residual water in DCM after the liquid−liquid extraction. The dielectric constant of the effective solvent system is increased by residual water that facilitates the reversible enamine formation between L-proline and heptanal.[72] The added polarity of the solvent system raises the highest occupied molecular orbital (HOMO) and the nucleophilicity of the resulting enamine.[72] Additionally, multiple turnover in the enamine catalysis cycle is conditional on its reversibility, which is prompted by the residual presence of water (Scheme S3).[71] Considering the higher reactivity of aldehydes than ketones and that diethyl azodicarboxylate (DEAD) is the limiting substrate in step III, it is expected that competing enamine formation between DEAD and the acetone used as cosolvent in step I is negligible.

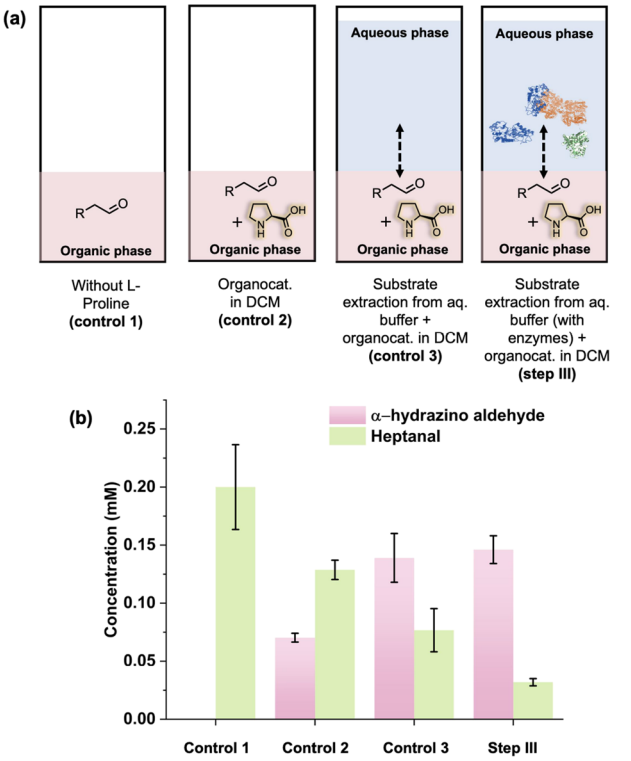

Figure 6. (a) Schematic representation of experimental control 1 wherein all organocatalytic conditions except L-proline were provided, control 2 wherein organocatalysis was conducted in DCM using heptanal stock, experimental control 3 wherein organocatalysis was conducted in DCM following heptanal extraction from the aqueous buffer (in the absence of alkG, alkB, $AcCO_6$, and catalase), and step III wherein organocatalysis was conducted in DCM following heptanal extraction from the aqueous buffer (in the presence of alkG, alkB, and $AcCO_6$). (b) Concentration profiles of heptanal and α-hydrazino aldehyde in the corresponding setups. Buffer: 50 mM Kpi buffer (pH 8.0) containing 50 mM NaCl and 15% glycerol.

CONCLUSIONS

A "three-stage" system that couples a bioelectrocatalytic multienzyme cascade and organocatalysis was developed for the sequential conversion of a chemically inert terminal C−H in an alkane to an α-hydrazino aldehyde under mild conditions. Bioelectrocatalytic regioselective heptane oxidation to 1-heptanol and biocatalytic 1-heptanol oxidation to heptanal, respectively, recorded a faradaic efficiency of 44% at 2.5 h and a conversion ratio of 91% at 4.5 h. Organocatalytic amination of heptanal records a 73% conversion at the 19.5 h

https://doi.org/10.1021/acscatal.2c04003
ACS Catal. 2023, 13, 563−572

mark. Further analysis of the final reaction media profile will be required to determine its ability to be extended to products like amino aldehydes. The high conversion rates across each step are attributable to the streamlined design, which makes it a practical and scalable system. For instance, replacing cofactors required for step I with reductive energy, incorporating a custom-designed redox polymer, and choosing a cofactor-independent engineered enzyme for step II limit the entities in the aqueous reaction media. This controlled composition of the media enables the eventual separation of a synthetically important intermediate (i.e., aldehyde) by an in situ liquid−liquid extraction with minimal crossover by interfering species. Therefore, the bioelectrocatalytic multienzyme cascade is seamlessly coupled to an established organocatalytic reaction. Inadvertently, the in situ liquid−liquid transfer of heptanal from aqueous to organic media during the system operation increases the organocatalytic turnover.

Different catalytic elements brought together in this design hold many future possibilities. AQ-LPEI is a versatile redox polymer that can be adapted for C−H functionalization by different bioelectrocatalytic systems. For example, AQ derivatives are used in the industrial-scale synthesis of H_2O_2 via O_2 reduction (i.e., "anthraquinone H_2O_2 process").[73] AQ-LPEI can be coupled with a H_2O_2-dependent alkane hydroxylase for electroenzymatic conversion of small alkanes to regioselective alcohols.[74] Theoretical calculations of the activation and concentration overpotential contributions at the interface between the polymer modified electrode surface and the enzymes and substrates in solution during the bioelectrocatalytic step are instrumental in optimizing future cell setups. Additionally, anthraquinones are photoactive molecules (i.e., photosensitizers), which makes them also potentially viable photocatalysts in photo-multienzymatic cascades for C−H bond functionalization.[75] Due to enzyme promiscuity, the substrate scope for the bioelectrocatalytic multienzyme cascade in step I extends to many aliphatic and aromatic hydrocarbons, epoxidation, sulfoxidation, and demethylation.[17,18] Similarly, in step III, L-proline catalyzed aldol reactions for C−C bond formation between aldehydes instead of the C−N bond formation can further expand the synthetic target molecules attainable with this system.[43,72] Therefore, the modularity of this "three-stage" system can extend to synthesize consistently more complex targets within the same catalytic framework.

■ ASSOCIATED CONTENT

Data Availability Statement

All data underlying this study are available in the supplementary material and specific data sets are openly available at the University of Utah Hive at DOI: 10.7278/S50d-m87v-xesj.

Supporting Information

The Supporting Information is available free of charge at https://pubs.acs.org/doi/10.1021/acscatal.2c04003.

Chemicals, bacterial strains, and medium; synthesis of 1-(prop-2′-enyloxyl)-anthraquinone (**1**); synthesis of 1-(oxiranylmethyloxy)-anthraquinone (**2**); synthesis of anthra-9,10-quinone linear polyethyleneimine redox hydrogel (AQ-LPEI) (**3**); expression and purification of alkB; expression and purification of enzymes with His-tag; enzyme activity assays; DNA sequences and amino acid sequences of enzymes used in this study; electrochemical methods; biocatalytic conversion from alcohol to aldehyde; screening for optimal conditions for aldehyde conversion; organocatalytic step: conversion of heptanal in aqueous buffer (in the presence of enzymes) after being extracted to an organic phase; positive control for the organocatalytic step: conversion of heptanal in aqueous buffer (in the absence of enzymes) after being extracted to an organic phase; and GC analysis. Figures of ^{1}H NMR spectrum of the synthesized AQ-LPEI redox polymer; XPS survey scan of AQ-LPEI; XPS high-resolution N scan of AQ-LPEI redox polymer; (a) monomeric unit of the AQ-LPEI polymer synthesized; (b) a sample of the AQ-LPEI polymer synthesized and sealed under nitrogen gas; FT-IR spectrum of the AQ-LPEI redox polymer; UV−visible spectrum of the AQ-LPEI redox polymer powder; schematic diagram of the bulk electrolysis cells; ^{1}H NMR of synthesized diethyl 1-(1-oxoheptan-2-yl)-hydrazine-1,2-dicarboxylate (**4**) standard; ^{13}C NMR of synthesized diethyl 1-(1-oxoheptan-2-yl)hydrazine-1,2-dicarboxylate (**4**) standard; high-resolution mass spectrometry (ESI) exact mass calculated for synthesized diethyl 1-(1-oxoheptan-2-yl)hydrazine-1,2-dicarboxylate (**4**) standard; GC analyses of the (a) 1-heptanol standard and (b) heptanal standard; and the GC analyses of the L-proline catalyzed asymmetric amination of heptanal in step III. Schemes of projected two-proton-coupled two-electron transfer mechanism in anthraquinone; synthesis of diethyl 1-(1-oxoheptan-2-yl) hydrazine-1,2-dicarboxylate (**4**) standard; and potential mechanism during the organocatalysis step resulting in direct asymmetric enantioselective α-amination (PDF)

■ AUTHOR INFORMATION

Corresponding Authors

Hui Chen − *Department of Chemistry, University of Utah, Salt Lake City, Utah 84112, United States;* orcid.org/0000-0002-8944-0090; Email: Chen.Hui@utah.edu

Shelley D. Minteer − *Department of Chemistry, University of Utah, Salt Lake City, Utah 84112, United States;* orcid.org/0000-0002-5788-2249; Email: minteer@chem.utah.edu

Authors

N. Samali Weliwatte − *Department of Chemistry, University of Utah, Salt Lake City, Utah 84112, United States*

Tianhua Tang − *Department of Chemistry, University of Utah, Salt Lake City, Utah 84112, United States*

Complete contact information is available at: https://pubs.acs.org/10.1021/acscatal.2c04003

Author Contributions

†N.S.W. and H.C. contributed equally to this study.

Notes

The authors declare no competing financial interest.

■ ACKNOWLEDGMENTS

The authors gratefully acknowledge funding from the National Science Foundation Center for Synthetic Organic Electrochemistry (CHE2002158). This work made use of the University of Utah USTAR shared facilities supported, in part, by the MRSEC program of NSF under award no. DMR-1121252. The authors gratefully acknowledge Skylar Blank

from the Department of Chemistry, University of Utah, for his contribution in analyzing the NMR spectroscopy data for this study.

REFERENCES

(1) Wang, Y.; Hu, P.; Yang, J.; Zhu, Y.-A.; Chen, D. C−H bond Activation in Light Alkanes: A Theoretical Perspective. *Chem. Soc. Rev.* **2021**, *50*, 4299−4358.
(2) IEA, I. E. A. *The Future of the Petrochemicals*; IEA: Paris, 2018; p 132.
(3) Davies, H. M. L.; Morton, D. Recent Advances in C−H Functionalization. *J. Org. Chem.* **2016**, *81*, 343−350.
(4) Hartwig, J. F.; Larsen, M. A. Undirected, Homogeneous C−H Bond Functionalization: Challenges and Opportunities. *ACS Cent. Sci.* **2016**, *2*, 281−292.
(5) Yi, H.; Zhang, G.; Wang, H.; Huang, Z.; Wang, J.; Singh, A. K.; Lei, A. Recent Advances in Radical C−H Activation/Radical Cross-Coupling. *Chem. Rev.* **2017**, *117*, 9016−9085.
(6) Labinger, J. A.; Bercaw, J. E. Understanding and Exploiting C−H Bond Activation. *Nature* **2002**, *417*, 507−514.
(7) Hudzik, J. M.; Bozzelli, J. W.; Simmie, J. M. Thermochemistry of C7H16 to C10H22 Alkane Isomers: Primary, Secondary, and Tertiary C−H Bond Dissociation Energies and Effects of Branching. *J. Phys. Chem. A* **2014**, *118*, 9364−9379.
(8) Bergman, R. G. C−H Activation. *Nature* **2007**, *446*, 391−393.
(9) Hickey, D. P.; McCammant, M. S.; Giroud, F.; Sigman, M. S.; Minteer, S. D. Hybrid Enzymatic and Organic Electrocatalytic Cascade for the Complete Oxidation of Glycerol. *J. Am. Chem. Soc.* **2014**, *136*, 15917−15920.
(10) Ayala, M.; Torres, E. Enzymatic Activation of Alkanes: Constraints and Prospective. *Appl. Catal.* **2004**, *272*, 1−13.
(11) Chen, H.; Dong, F.; Minteer, S. D. The progress and outlook of bioelectrocatalysis for the production of chemicals, fuels and materials. *Nat. Catal.* **2020**, *3*, 225−244.
(12) Mahor, D.; Cong, Z.; Weissenborn, M. J.; Hollmann, F.; Zhang, W. Valorization of Small Alkanes by Biocatalytic Oxyfunctionalization. *ChemSusChem* **2022**, *15*, No. e202101116.
(13) Walsh, C. T.; Moore, B. S. Enzymatic Cascade Reactions in Biosynthesis. *Angew. Chem., Int. Ed.* **2019**, *58*, 6846−6879.
(14) Wender, P. A.; Miller, B. L. Synthesis at the Molecular Frontier. *Nature* **2009**, *460*, 197−201.
(15) Trost, B. The Atom Economy - A Search for Synthetic Efficiency. *Science* **1991**, *254*, 1471−1477.
(16) Yu, H.-L.; Li, T.; Chen, F.-F.; Luo, X.-J.; Li, A.; Yang, C.; Zheng, G.-W.; Xu, J.-H. Bioamination of Alkane with Ammonium by an Artificially Designed Multienzyme Cascade. *Metab. Eng.* **2018**, *47*, 184−189.
(17) Yuan, M.; Abdellaoui, S.; Chen, H.; Kummer, M. J.; Malapit, C. A.; You, C.; Minteer, S. D. Selective Electroenzymatic Oxy-functionalization by Alkane Monooxygenase in a Biofuel Cell. *Angew. Chem., Int. Ed.* **2020**, *59*, 8969−8973.
(18) Chen, H.; Tang, T.; Malapit, C. A.; Lee, Y. S.; Prater, M. B.; Weliwatte, N. S.; Minteer, S. D. One-Pot Bioelectrocatalytic Conversion of Chemically Inert Hydrocarbons to Imines. *J. Am. Chem. Soc.* **2022**, *144*, 4047−4056.
(19) Giroud, F.; Milton, R. D.; Tan, B.-X.; Minteer, S. D. Simplifying Enzymatic Biofuel Cells: Immobilized Naphthoquinone as a Biocathodic Orientational Moiety and Bioanodic Electron Mediator. *ACS Catal.* **2015**, *5*, 1240−1244.
(20) Mazurenko, I.; Hitaishi, V. P.; Lojou, E. Recent Advances in Surface Chemistry of Electrodes to Promote Direct Enzymatic Bioelectrocatalysis. *Curr. Opin. Electrochem.* **2020**, *19*, 113−121.
(21) Zhang, W.; Hollmann, F. Nonconventional Regeneration of Redox Enzymes − A Practical Approach for Organic Synthesis? *Chem. Commun.* **2018**, *54*, 7281−7289.
(22) Castañeda-Losada, L.; Adam, D.; Paczia, N.; Buesen, D.; Steffler, F.; Sieber, V.; Erb, T. J.; Richter, M.; Plumeré, N. Bioelectrocatalytic Cofactor Regeneration Coupled to CO_2 Fixation in a Redox-Active Hydrogel for Stereoselective C−C Bond Formation. *Angew. Chem., Int. Ed.* **2021**, *60*, 21056−21061.
(23) Heller, A. Electron-Conducting Redox Hydrogels: Design, Characteristics and Synthesis. *Curr. Opin. Chem. Biol.* **2006**, *10*, 664−672.
(24) Andrieux, C. P.; Savéant, J. M. Kinetics of Electrochemical Reactions Mediated by Redox Polymer Films: Pre-activation (CE) Mechanisms. *J. Electroanal. Chem. Interfacial Electrochem.* **1984**, *171*, 65−93.
(25) Yuan, M.; Minteer, S. D. Redox Polymers in Electrochemical Systems: From Methods of Mediation to Energy Storage. *Curr. Opin. Electrochem.* **2019**, *15*, 1−6.
(26) Ruff, A. Redox Polymers in Bioelectrochemistry: Common Playgrounds and Novel Concepts. *Curr. Opin. Electrochem.* **2017**, *5*, 66−73.
(27) Yuan, M.; Sahin, S.; Cai, R.; Abdellaoui, S.; Hickey, D. P.; Minteer, S. D.; Milton, R. D. Creating a Low-Potential Redox Polymer for Efficient Electroenzymatic CO_2 Reduction. *Angew. Chem., Int. Ed.* **2018**, *57*, 6582−6586.
(28) Kuk, S. K.; Gopinath, K.; Singh, R. K.; Kim, T.-D.; Lee, Y.; Choi, W. S.; Lee, J.-K.; Park, C. B. NADH-Free Electroenzymatic Reduction of CO_2 by Conductive Hydrogel-Conjugated Formate Dehydrogenase. *ACS Catal.* **2019**, *9*, 5584−5589.
(29) Szczesny, J.; Ruff, A.; Oliveira, A. R.; Pita, M.; Pereira, I. A. C.; De Lacey, A. L.; Schuhmann, W. Electroenzymatic CO_2 Fixation Using Redox Polymer/Enzyme-Modified Gas Diffusion Electrodes. *ACS Energy Lett.* **2020**, *5*, 321−327.
(30) Denard, C. A.; Huang, H.; Bartlett, M. J.; Lu, L.; Tan, Y.; Zhao, H.; Hartwig, J. F. Cooperative Tandem Catalysis by an Organometallic Complex and a Metalloenzyme. *Angew. Chem., Int. Ed.* **2014**, *53*, 465−469.
(31) Freakley, S. J.; Kochius, S.; van Marwijk, J.; Fenner, C.; Lewis, R. J.; Baldenius, K.; Marais, S. S.; Opperman, D. J.; Harrison, S. T. L.; Alcalde, M.; Smit, M. S.; Hutchings, G. J. A Chemo-enzymatic Oxidation Cascade to Activate C−H Bonds with in situ Generated H2O2. *Nat. Commun.* **2019**, *10*, 4178.
(32) Craven, E. J.; Latham, J.; Shepherd, S. A.; Khan, I.; Diaz-Rodriguez, A.; Greaney, M. F.; Micklefield, J. Programmable Late-Stage C−H Bond Functionalization Enabled by Integration of Enzymes with Chemocatalysis. *Nat. Catal.* **2021**, *4*, 385−394.
(33) Sperl, J. M.; Sieber, V. Multienzyme Cascade Reactions—Status and Recent Advances. *ACS Catal.* **2018**, *8*, 2385−2396.
(34) Denard, C. A.; Bartlett, M. J.; Wang, Y.; Lu, L.; Hartwig, J. F.; Zhao, H. Development of a One-Pot Tandem Reaction Combining Ruthenium-Catalyzed Alkene Metathesis and Enantioselective Enzymatic Oxidation to Produce Aryl Epoxides. *ACS Catal.* **2015**, *5*, 3817−3822.
(35) Rudroff, F.; Mihovilovic, M. D.; Gröger, H.; Snajdrova, R.; Iding, H.; Bornscheuer, U. T. Opportunities and Challenges for Combining Chemo- and Biocatalysis. *Nat. Catal.* **2018**, *1*, 12−22.
(36) Li, Y.; Yuan, B.; Sun, Z.; Zhang, W. C−H Bond Functionalization Reactions Enabled by Photobiocatalytic Cascades. *Green Synth. Catal.* **2021**, *2*, 267−274.
(37) Cai, J.; Zhao, L.; Li, Y.; He, C.; Wang, C.; Duan, C., Binding of Dual-Function Hybridized Metal−Organic Capsules to Enzymes for Cascade Catalysis. JACS Au2022, *2*, 1736 −1746, DOI: 10.1021/jacsau.2c00322.
(38) Katopodis, A. G.; Smith, H. A.; May, S. W. New oxyfunctionalization capabilities for. omega.-hydroxylases. Asymmetric aliphatic sulfoxidation and branched ether demethylation. *J. Am. Chem. Soc.* **1988**, *110*, 897−899.
(39) Heath, R. S.; Birmingham, W. R.; Thompson, M. P.; Taglieber, A.; Daviet, L.; Turner, N. J. An engineered alcohol oxidase for the oxidation of primary alcohols. *ChemBioChem* **2019**, *20*, 276−281.
(40) Bol, D. K.; Yasbin, R. E. The isolation, cloning and identification of a vegetative catalase gene from *Bacillus subtilis*. *Gene* **1991**, *109*, 31−37.
(41) Sanderson, K. Amino Acid Provides Shortcut to Drugs. *Nature* **2012**, *488*, 266−266.

(42) Marigo, M.; Jørgensen, K. A. Organocatalytic Direct Asymmetric α-Heteroatom Functionalization of Aldehydes and Ketones. *Chem. Commun.* **2006**, 2001−2011.
(43) List, B. Enamine Catalysis is a Powerful Strategy for the Catalytic Generation and use of Carbanion Equivalents. *Acc. Chem. Res.* **2004**, *37*, 548−557.
(44) Zarren, G.; Nisar, B.; Sher, F. Synthesis of Anthraquinone-Based Electroactive Polymers: A Critical Review. *Mater. Today Sustainability* **2019**, *5*, No. 100019.
(45) Sarapuu, A.; Helstein, K.; Vaik, K.; Schiffrin, D. J.; Tammeveski, K. Electrocatalysis of Oxygen Reduction by Quinones Adsorbed on Highly-Oriented Pyrolytic Graphite Electrodes. *Electrochim. Acta* **2010**, *55*, 6376−6382.
(46) Huskinson, B.; Marshak, M. P.; Suh, C.; Er, S.; Gerhardt, M. R.; Galvin, C. J.; Chen, X.; Aspuru-Guzik, A.; Gordon, R. G.; Aziz, M. J. A Metal-Free Organic−Inorganic Aqueous Flow Battery. *Nature* **2014**, *505*, 195−198.
(47) Adachi, M.; Shimomura, T.; Komatsu, M.; Yakuwa, H.; Miya, A. A Novel Mediator−Polymer-Modified Anode for Microbial Fuel Cells. *Chem. Commun.* **2008**, 2055−2057.
(48) Xu, N.; Wang, T.-L.; Li, W.-J.; Wang, Y.; Chen, J.-J.; Liu, J. Tuning Redox Potential of Anthraquinone-2-Sulfonate (AQS) by Chemical Modification to Facilitate Electron Transfer From Electrodes in Shewanella oneidensis. *Front. Bioeng. Biotechnol.* **2021**, *9*, No. 705414.
(49) Blanchard, P. Y.; Buzzetti, P. H. M.; Davies, B.; Nedellec, Y.; Girotto, E. M.; Gross, A. J.; Le Goff, A.; Nishina, Y.; Cosnier, S.; Holzinger, M. Electrosynthesis of pyrenediones on carbon nanotube electrodes for efficient electron transfer with FAD-dependent glucose dehydrogenase in biofuel cell anodes. *ChemElectroChem* **2019**, *6*, 5242−5247.
(50) Martínez, M. J. A.; Benito, P. B., Biological Activity of Quinones. In *Studies in Natural Products Chemistry*; Attaur, R., Ed.; Elsevier: 2005, Vol. *30*; pp 303−366.
(51) Weliwatte, N. S.; Grattieri, M.; Minteer, S. D. Rational Design of Artificial Redox-Mediating Systems toward Upgrading Photobioelectrocatalysis. *Photochem. Photobiol. Sci.* **2021**, *20*, 1333−1356.
(52) Ma, W.; Long, Y.-T. Quinone/Hydroquinone-Functionalized Biointerfaces for Biological Applications from the Macro- to Nanoscale. *Chem. Soc. Rev.* **2014**, *43*, 30−41.
(53) Wahyuni, W. T.; Putra, B. R.; Harito, C.; Bavykin, D. V.; Walsh, F. C.; Fletcher, P. J.; Marken, F. Extraction of Hydrophobic Analytes from Organic Solution into a Titanate 2D-Nanosheet Host: Electroanalytical Perspectives. *Anal. Chim. Acta: X* **2019**, *1*, No. 100001.
(54) El-Najjar, N.; Gali-Muhtasib, H.; Vuorela, P.; Urtti, A.; Vuorela, H. Naphthoquinones and Anthraquinones: Chemical, Analytical, and Biological Overview. In *Encyclopedia of Analytical Chemistry*; 2014; pp 1 −16.
(55) An, N.; Zhang, F.; Hu, Z.; Li, Z.; Li, L.; Yang, Y.; Guo, B.; Lei, Z. Non-covalently Functionalizing a Graphene Framework by Anthraquinone for High-Rate Electrochemical Energy Storage. *RSC Adv.* **2015**, *5*, 23942−23951.
(56) Yuan, W.; Li, H., Polymer-Based Nanocarriers for Therapeutic Nucleic Acids Delivery. In *Nanostructures for Drug Delivery*; Andronescu, E., Grumezescu, A. M., Eds.; Elsevier, 2017; pp 445−460.
(57) Macazo, F. C.; Hickey, D. P.; Abdellaoui, S.; Sigman, M. S.; Minteer, S. D. Polymer-Immobilized, Hybrid Multi-Catalyst Architecture for Enhanced Electrochemical Oxidation of Glycerol. *Chem. Commun.* **2017**, *53*, 10310−10313.
(58) Mao, F.; Mano, N.; Heller, A. Long Tethers Binding Redox Centers to Polymer Backbones Enhance Electron Transport in Enzyme "Wiring" Hydrogels. *J. Am. Chem. Soc.* **2003**, *125*, 4951−4957.
(59) Milton, R. D.; Hickey, D. P.; Abdellaoui, S.; Lim, K.; Wu, F.; Tan, B.; Minteer, S. D. Rational Design of Quinones for High Power Density Biofuel Cells. *Chem. Sci.* **2015**, *6*, 4867−4875.
(60) Song, N.; Gagliardi, C. J.; Binstead, R. A.; Zhang, M.-T.; Thorp, H.; Meyer, T. J. Role of Proton-Coupled Electron Transfer in the Redox Interconversion between Benzoquinone and Hydroquinone. *J. Am. Chem. Soc.* **2012**, *134*, 18538−18541.
(61) Mano, N.; Soukharev, V.; Heller, A. A Laccase-Wiring Redox Hydrogel for Efficient Catalysis of O2 Electroreduction. *J. Phys. Chem. B* **2006**, *110*, 11180−11187.
(62) Zahn, R.; Coullerez, G.; Vörös, J.; Zambelli, T. Effect of Polyelectrolyte Interdiffusion on Electron Transport in Redox-Active Polyelectrolyte Multilayers. *J. Mater. Chem.* **2012**, *22*, 11073−11078.
(63) Miller, L. L.; Zinger, B.; Degrand, C. The Effects of Cross-Linking and Anodic Surface Roughening on Quinone Polymer/Carbon Electrodes. *J. Electroanal. Chem. Interfacial Electrochem.* **1984**, *178*, 87−99.
(64) Fukui, M.; Kitani, A.; Degrand, C.; Miller, L. L. Propagation of a Redox Reaction Through a Quinoid Polymer Film on an Electrode. *J. Am. Chem. Soc.* **1982**, *104*, 28−33.
(65) Zhao, J.; Hernández, W. Y.; Zhou, W.; Yang, Y.; Vovk, E. I.; Capron, M.; Ordomsky, V. Selective Oxidation of Alcohols to Carbonyl Compounds over Small Size Colloidal Ru Nanoparticles. *ChemCatChem* **2020**, *12*, 238−247.
(66) Enache, D. I.; Edwards, J. K.; Landon, P.; Solsona-Espriu, B.; Carley, A. F.; Herzing, A. A.; Watanabe, M.; Kiely, C. J.; Knight, D. W.; Hutchings, G. J. Solvent-Free Oxidation of Primary Alcohols to Aldehydes Using Au-Pd/TiO_2 Catalysts. *Science* **2006**, *311*, 362−365.
(67) Silva, T. F. S.; Martins, L. M. D. R. S. Recent Advances in Copper Catalyzed Alcohol Oxidation in Homogeneous Medium. *Molecules* **2020**, *25*, 748.
(68) Evans, D. A. Stereoselective Organic Reactions: Catalysts for Carbonyl Addition Processes. *Science* **1988**, *240*, 420−426.
(69) Duthaler, R. O. Proline-Catalyzed Asymmetric α-Amination of Aldehydes and Ketones—An Astonishingly Simple Access to Optically Active α-Hydrazino Carbonyl Compounds. *Angew. Chem., Int. Ed.* **2003**, *42*, 975−978.
(70) Bøgevig, A.; Juhl, K.; Kumaragurubaran, N.; Zhuang, W.; Jørgensen, K. A. Direct Organo-Catalytic Asymmetric α-Amination of Aldehydes—A Simple Approach to Optically Active α-Amino aldehydes, α-amino alcohols, and α-amino acids. *Angew. Chem., Int. Ed.* **2002**, *41*, 1790−1793.
(71) List, B. Direct Catalytic Asymmetric α-Amination of Aldehydes. *J. Am. Chem. Soc.* **2002**, *124*, 5656−5657.
(72) Mukherjee, S.; Yang, J. W.; Hoffmann, S.; List, B. Asymmetric Enamine Catalysis. *Chem. Rev.* **2007**, *107*, 5471−5569.
(73) Korth, H.-G.; Mulder, P. Phenolic Hydrogen Transfer by Molecular Oxygen and Hydroperoxyl Radicals: Insights into the Mechanism of the Anthraquinone Process. *J. Org. Chem.* **2020**, *85*, 2560−2574.
(74) Chen, J.; Kong, F.; Ma, N.; Zhao, P.; Liu, C.; Wang, X.; Cong, Z. Peroxide-Driven Hydroxylation of Small Alkanes Catalyzed by an Artificial P450BM3 Peroxygenase System. *ACS Catal.* **2019**, *9*, 7350−7355.
(75) Cervantes-González, J.; Vosburg, D. A.; Mora-Rodriguez, S. E.; Vázquez, M. A.; Zepeda, L. G.; Villegas Gómez, C.; Lagunas-Rivera, S. Anthraquinones: Versatile Organic Photocatalysts. *ChemCatChem* **2020**, *12*, 3811−3827.

https://doi.org/10.1021/acscatal.2c04003
ACS Catal. 2023, 13, 563−572